Rounded-corners-induced re-entrant non-occlusion in a horizontal tube

Dongwen Tan[1] and Xinping Zhou[1,2,]†
[1]School of Mechanical Science and Engineering, Huazhong University of Science and Technology, Wuhan 430074, PR China
[2]State Key Laboratory of Intelligent Manufacturing Equipment and Technology, Huazhong University of Science and Technology, Wuhan 430074, PR China
†Email address for correspondence: xpzhou08@hust.edu.cn (X. Zhou)

Supplementary Information

1. Geometry and constraints

We here use Surface Evolver (SE) (Brakke 2011) to calculate the occluding capillary surface in a horizontal tube with only one rounded corner in a downward gravity field. SE software minimizes the energy of a capillary surface subject to constraints by using the gradient descent method. Starting with the initial state, the surface which is discretized into a set of triangular facets is evolved down the energy gradient with each iteration of SE. After enough iterations, the surface can reach the minimum energy state (if it exists), in which the surface is regarded as an equilibrium surface.

The tube cross-section with only one rounded corner at the orientation angle of 90º is considered and shown in figure S1(*a*). The perimeter consists of a primary circle arc with the radius R, a rounded corner arc with the radius r and two straight edges forming an angle α. The distance between the centre of the primary circle and the centre of the rounded corner arc is d.

For the tube with the cross-section shown in figure S1(*a*), Chen (2003) studied the occluding surface in zero gravity by SE modeling. Though a downward gravity field is considered here, we refer to the settings of geometrical constraints of Chen (2003), which are independent of gravity. The occluding surface in the tube is supposed to be symmetric with aspect to the vertical plane of symmetry in a downward gravity field. Thus, a symmetrical plane constraint is used on SE modeling to reduce computational time. The model skeleton of SE under the symmetrical plane constraint is shown in figure S1(*b*), which is in the plane $z = 0$.

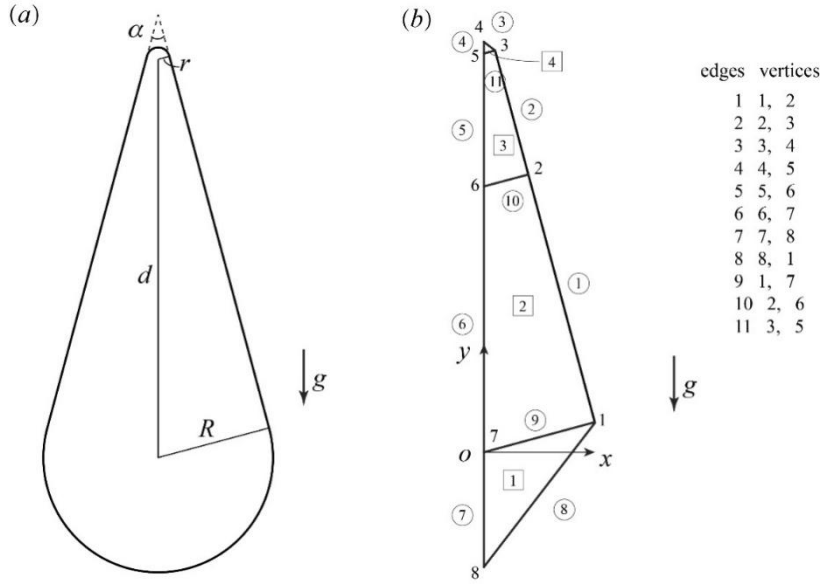

Figure S1. (a) Cross-section of a tube with one rounded corner. (b) The model skeleton.

We prescribe the radius of the primary circle to be 1, then have $d = (1-r)/\sin(\alpha/2)$.

The geometry for SE modeling includes four parts, i.e. the primary circle (edge 8), the rounded corner (edge 3), the straight edge (edges 1, 2) and the symmetrical plane (edge 4, 5, 6, 7). The geometrical functions for these parts can be expressed as

$$\text{the primary circle:} \quad x^2 + y^2 = 1, \tag{1}$$

$$\text{the rounded corner:} \quad x^2 + (y-d)^2 = r^2, \tag{2}$$

$$\text{the straight edge:} \quad y\sin\frac{\alpha}{2} + x\cos\frac{\alpha}{2} = 1, \tag{3}$$

$$\text{the symmetrical plane:} \quad y = 0. \tag{4}$$

For the junction points (vertices 1, 3) between the curve boundaries (the primary circle and the rounded corner) and the straight edge, constraints are imposed to fix the *x*-coordinates and *y*-coordinates, i.e. $x = \cos(\alpha/2)$ and $y = \sin(\alpha/2)$ for vertex 1, and $x = r\cos(\alpha/2)$ and $y = r\sin(\alpha/2) + d$ for vertex 3. Besides, one-sided constrains are applied to the straight edge to keep the liquid on the straight edge in the range of $y = \sin(\alpha/2)$ to $y = r\sin(\alpha/2) + d$. To keep the vertices on the wall of rounded corner evenly spaced, a periodic constraint is applied to the rounded corner.

A virtual base for the tube is assumed to exist at z = 0, which only serves as a supplementary surface when using the Divergence theorem or Stokes' theorem to derive the constraint energy/volume integrands. The virtual base dose not limit the surface motion. The volume of liquid can be set to 0, because the volume only affects the position of the surface in the *z* direction but does not affect the shape of the surface.

2. Constraint energy/volume integrands

For derivation on the constraint energy/volume integrands, we mainly refer to the Example 7 of the Tutorial in the SE Manual (Brakke 2011). In this research, the total energy to be minimized includes the liquid-gas interface energy E_I, the wetting energy E_W and the gravitational potential energy E_G. Besides, the energy minimization is subject to the liquid volume V. We will derive the integrands corresponding to E_I, E_W, E_G and V independently.

2.1 Interface energy

The liquid-gas interface energy E_I is automatically calculated by SE. Because the primary circle and the rounded corner are curve boundary, gap exists between the facets edge and the wall. We should declare the boundary of primary circle and rounded to be CONVEX so that SE will include the gap interface energy.

2.2 Wetting energy

The wetting energy E_W can be divided into three parts, namely the part on the wall of primary circle, the part on the wall of rounded corner and the part on the wall of straight edge. Then, E_W can be expressed as

$$E_W = -\cos\gamma \iint_{D_{pc}} \vec{n}_{pc} \cdot \mathrm{d}\vec{A} - \cos\gamma \iint_{D_{rc}} \vec{n}_{rc} \cdot \mathrm{d}\vec{A} - \cos\gamma \iint_{D_{se}} \vec{n}_{se} \cdot \mathrm{d}\vec{A} \tag{5}$$

where $\vec{n}$ denotes the unit exterior normal to the wall, and the subscripts *pc*, *rc* and *se* denote the primary circle, the rounded corner, and the straight edge, respectively. Note that the symmetrical plane and the virtual base are ignored when calculating the wetting

energy by assuming the contact angle to be 90º. The surface tension coefficient σ is set by default to 1 in SE and used in (5) and the following expressions.

By using Stokes' theorem, the wetting energy of each part will be respectively transformed into line integral and then the constraint energy integrands for edges will be obtained. For the primary circle part, the wetting energy has the relationship

$$-\cos\gamma\iint_{D_{pc}}\vec{n}_{pc}\cdot\mathrm{d}\vec{A}=-\cos\gamma\iint_{D_{pc}}\vec{F}_{pc}\cdot\mathrm{d}\vec{A}=-\cos\gamma\int_{L_{pc\_cl}}\vec{w}_{pc}\cdot\mathrm{d}\vec{s}, \tag{6}$$

where $\vec{F}$ is a divergenceless integrand and $\vec{w}$ is the vector potential of $\vec{F}$. Based on the geometrical function of the primary circle, $\vec{F}_{pc}$ can be constructed as

$$\vec{F}_{pc}=\frac{1}{x^2+y^2}\left(x\vec{i}+y\vec{j}\right). \tag{7}$$

Then, $\vec{w}$ can be given by

$$\vec{w}_{pc}=\frac{z}{x^2+y^2}\left(y\vec{i}-x\vec{j}\right),\quad \nabla\times\vec{w}_{pc}=\vec{F}_{pc}. \tag{8}$$

A gap exists between the contact line on the wall of primary circle and the facet edge. However, since $\nabla\times\vec{w}_{pc}$ is parallel to the gap surface, we have

$$\int_{L_{pc\_cl}}\vec{w}_{pc}\cdot\mathrm{d}\vec{s}=\int_{L_{pc\_edge}}\vec{w}_{pc}\cdot\mathrm{d}\vec{s}, \tag{9}$$

where the subscript *pc_edge* denotes the edges of facets on the wall of the primary circle. Considering the integral orientation opposite to the orientation of edge 8, we include $\cos\gamma\vec{w}_{pc}$ in the energy integrand on edge 8.

Similarly, for the wetting energy on the rounded corner part, we have the relationship

$$-\cos\gamma\iint_{D_{rc}}\vec{n}_{rc}\cdot\mathrm{d}\vec{A}=-\cos\gamma\iint_{D_{rc}}\vec{F}_{rc}\cdot\mathrm{d}\vec{A}=-\cos\gamma\int_{L_{rc\_cl}}\vec{w}_{pc}\cdot\mathrm{d}\vec{s}, \tag{10}$$

where the subscript *rc_cl* denotes the contact line on the wall of rounded corner part. $\vec{F}_{rc}$ and $\vec{w}_{pc}$ can be constructed as

$$\vec{F}_{rc}=\frac{r}{x^2+(y-d)^2}\left(x\vec{i}+(y-d)\vec{j}\right), \tag{11}$$

$$\vec{w}_{rc}=\frac{rz}{x^2+(y-d)^2}\left((y-d)\vec{i}-x\vec{j}\right),\quad \nabla\times\vec{w}_{rc}=\vec{F}_{rc}, \tag{12}$$

respectively. Considering the integral orientation opposite to the orientation of edge 3, we include $\cos\gamma\vec{w}_{rc}$ in the energy integrand on edge 3.

For the wetting energy on the wall of straight edge, we have the relationship

$$-\cos\gamma\iint_{D_{se}}\vec{n}_{se}\cdot\mathrm{d}\vec{A}=-\cos\gamma\int_{L_{se\_cl}}\vec{w}_{se}\cdot\mathrm{d}\vec{s}, \tag{13}$$

where the subscript *se_cl* is the contact line on the wall of straight edge. $\vec{n}_{se}$ and $\vec{w}_{se}$ can be expressed as

$$\vec{n}_{se}=\cos(\alpha/2)\vec{i}+\sin(a/2)\vec{j}, \tag{14}$$

$$\vec{w}_{se}=z\sin(\alpha/2)\vec{i}-z\cos(a/2)\vec{j},\quad \nabla\times\vec{w}_{se}=\vec{n}_{se}. \tag{15}$$

respectively. Considering the integral orientation opposite the orientations of edges 1 and 2, we include $\cos\gamma\vec{w}_{se}$ in the energy integrand on edges 1 and 2.

2.3 Gravitational potential energy

The gravity in this case is along the negative *y* direction. Based on the Divergence theorem,

we have the relationship of gravitational potential energy of the liquid as

$$E_G = \iiint_{body} \rho g y \mathrm{d}V = \iint_{\partial body} \rho g \vec{F}_G \cdot d\vec{A}, \quad \vec{F}_G = yz\vec{k}. \tag{16}$$

The boundary surface of the liquid body includes the liquid-gas interface, the wetting wall, the symmetric plane, and the virtual base. Only the liquid-gas interface needs to be taken into consideration for the calculation on (16), because the integrand $\vec{F}_G = yz\vec{k}$ is parallel to the wetting wall and the symmetric plane, and because $\vec{F}_G = 0$ on the virtual base ($z = 0$),

The liquid-gas interface part consists of the facets and the gaps. A named quantity about gravity is defined for the facets, in which the integrand is $\rho g \vec{F}_G$. The gaps exist between the primary circle wall and the facet edge, and between the rounded corner wall and the facet edge.

For the gaps on the primary circle, an equivalent divergence-free integrand to $\vec{F}_G$ can be constructed as

$$\vec{F}_{E\_pc} = \vec{F}_G - \frac{yx}{3}\vec{i} - \frac{y^2}{3}\vec{j} = -\frac{yx}{3}\vec{i} - \frac{y^2}{3}\vec{j} + yz\vec{k}, \tag{17}$$

where the subscript *E_pc* means the equivalent integrand to $\vec{F}_G$ for the gaps on the primary circle wall. As the added vector $(-\frac{yx}{3}\vec{i} - \frac{y^2}{3}\vec{j})$ is parallel to the gaps, $\vec{F}_{E\_pc}$ is equivalent to $\vec{F}_G$ when calculating (16) for the gaps. Then the vector potential of $\vec{F}_{E\_pc}$ can be given by

$$\vec{w}_{E\_pc} = \frac{yz}{3}(-y\vec{i} + x\vec{j}), \quad \nabla \times \vec{w}_{E\_pc} = \vec{F}_{E\_pc}. \tag{18}$$

$\vec{w}_{E\_pc}$ is integrated over the gap edge on the primary circle wall in the negative orientation on edge 8. For the contact line on the primary circle wall, based on the boundary function of the primary circle, we can construct an equivalent vector with radial curl as

$$\vec{w}_{E\_pc\_r} = \frac{yz}{3}\frac{1}{(x^2+y^2)^{\frac{3}{2}}}(-y\vec{i} + x\vec{j}). \tag{19}$$

Thus, we have

$$\int_{L_{pc\_cl}} \vec{w}_{E\_pc\_r} \cdot \mathrm{d}\vec{s} = \int_{L_{pc\_edge}} \vec{w}_{E\_pc\_r} \cdot \mathrm{d}\vec{s}. \tag{20}$$

$\vec{w}_{E\_pc\_r}$ is integrated over the gap edge on the primary circle wall in the same orientation on edge 8. Then, we include $\rho g(\vec{w}_{E\_pc\_r} - \vec{w}_{E\_pc})$ in the energy integrand on edge 8.

For the gaps on the rounded corner wall, an equivalent divergence-free integrand to $\vec{F}_G$ can be constructed as

$$\vec{F}_{E\_rc} = \left(-\frac{(y-d)x}{3}\vec{i} - \frac{(y-d)^2}{3}\vec{j} + (y-d)z\vec{k}\right) + d\left(-\frac{x}{2}\vec{i} - \frac{y-d}{2}\vec{j} + z\vec{k}\right), \tag{21}$$

where the subscript *E_rc* means the equivalent integrand to $\vec{F}_G$ for the gaps of the rounded corner part. Then the vector potential of $\vec{F}_{E\_rc}$ can be given by

$$\vec{w}_{E\_rc} = \frac{(y-d)z}{3}\left(-(y-d)\vec{i} + x\vec{j}\right) + \frac{dz}{2}\left(-(y-d)\vec{i} + x\vec{j}\right). \tag{22}$$

$\vec{w}_{E\_rc}$ is integrated over the gap edge on the rounded wall in the negative orientation on edge 3. For the contact line on the rounded circle wall, based on the boundary function of the rounded circle, we can construct an equivalent vector with radial curl as

$$\vec{w}_{E\_rc\_r} = \frac{(y-d)z}{3}\frac{r^3}{(x^2+(y-d)^2)^{\frac{3}{2}}}\left(-(y-d)\vec{i} + x\vec{j}\right) + \frac{dz}{2}\frac{r^2}{x^2+(y-d)^2}\left(-(y-d)\vec{i} + x\vec{j}\right). \tag{23}$$

Thus, we have

$$\int_{L_{rc\_cl}} \vec{w}_{E\_rc\_r} \cdot \mathrm{d}\vec{s} = \int_{L_{rc\_edge}} \vec{w}_{E\_rc\_r} \cdot \mathrm{d}\vec{s}. \tag{24}$$

$\vec{w}_{E\_rc\_r}$ is integrated over the gap edge on the primary circle wall in the same orientation on edge 3. Then, we include $\rho g(\vec{w}_{E\_rc\_r} - \vec{w}_{E\_rc})$ in the energy integrand on edge 3.

2.4. Volume

For the liquid body volume, we have the relationship

$$V = \iiint_{body} \mathrm{d}V = \iint_{\partial body} \vec{F}_V \cdot d\vec{A}, \quad \vec{F}_V = z\vec{k}. \tag{25}$$

Similar to (17), the only portion needed to be considered is the liquid-gas interface. The liquid-gas interface including two parts i.e. the facets and the gaps. The volume calculation for the part of facets is conduct automatically by SE. The gaps exist on the wall of primary circle and on the wall of the rounded corner.

For the gaps of primary circle, we constructed a divergenceless vector to $\vec{F}_V$ as

$$\vec{F}_{V\_pc} = -\frac{x}{2}\vec{i} - \frac{y}{2}\vec{j} + z\vec{k}, \tag{26}$$

where the subscript *V_pc* means the equivalent and divergenceless integrand to $\vec{F}_V$ for the gaps of the primary circle part. The vector potential of $\vec{F}_{V\_pc}$ is given by

$$\vec{w}_{V\_pc} = -\frac{yz}{2}\vec{i} + \frac{xz}{2}\vec{j}, \quad \nabla \times \vec{w}_{V\_pc} = \vec{F}_{V\_pc}. \tag{27}$$

$\vec{w}_{V\_pc}$ is integrated over the gap edge on the rounded wall in the negative orientation on edge 8. For the contact line on the primary circle, we can construct an equivalent vector with radial curl as

$$\vec{w}_{V\_pc\_r} = \frac{z}{2(x^2+y^2)}(-y\vec{i} + x\vec{j}), \tag{28}$$

which is integrated over the gap edge on the rounded wall in the same orientation on edge 8. Thus, we include $(\vec{w}_{V\_pc\_r} - \vec{w}_{V\_pc})$ in the volume integrand on edge 8.

Similarly, for the gaps of rounded, the divergenceless form of $\vec{F}_V$ is given by

$$\vec{F}_{V\_rc} = -\frac{x}{2}\vec{i} - \frac{y-d}{2}\vec{j} + z\vec{k}, \tag{29}$$

where the subscript *V_rc* means the equivalent and divergenceless integrand to $\vec{F}_V$ for the gaps of the rounded corner part. Then, the vector potential and its equivalent vector with radial curl are constructed as

$$\vec{w}_{V\_rc} = -\frac{(y-d)z}{2}\vec{i} + \frac{xz}{2}\vec{j}, \tag{30}$$

$$\vec{w}_{V\_rc\_r} = \frac{zr^2}{2(x^2+(y-d)^2)}(-(y-d)\vec{i} + x\vec{j}), \tag{31}$$

respectively. $\vec{w}_{V\_rc}$ is integrated in the negative orientation on edge 3, while $\vec{w}_{V\_rc\_r}$ is integrated in the same orientation on edge 3. Thus, we include $(\vec{w}_{V\_rc\_r} - \vec{w}_{V\_rc})$ in the volume integrand on edge 3.

3. Results

The SE results for the case of $\alpha = 30°$ and $r = 0.1$ with $\gamma = 55°$ at different Bond numbers are presented in this section. The lower critical Bond number Bo_{cl} and upper critical Bond number Bo_{cu} for this case are theoretically determined to be $Bo_{cl} = 0.2474$ and $Bo_{cu} = 0.8183$, respectively.

The starting geometry for SE modeling is shown in figure S1 (*a*). Besides the overall refinement (SE command: *r*), the partial refinement (such as SE command: refine edges where lengths > 0.3) is performed during the computation, which is mainly to refine the stretched part of the interface. Vertex averaging (SE command: V), equiangulation (SE command: u) and trimming (SE command: t) are also performed during the computation. Some examples of the solutions for SE modeling can be seen in figure S2(*b*-*e*). Only half of the interface is computed due to the symmetry of the geometry. The other half of the interface can be generated by mirroring the half computed, and then the complete interface can be obtained such as shown in figure 3(*b*) and figure 4(*a*) in the maintext.

The interface axial length can be expressed as

$$l_z = z^s_{max} - z^s_{min}, \tag{32}$$

where z^s_{max} and z^s_{min} denote the maximum and minimum z values of the points on the symmetry plane, respectively. We take l_z as an indicator to investigate the grid independence and the convergence of the SE computation.

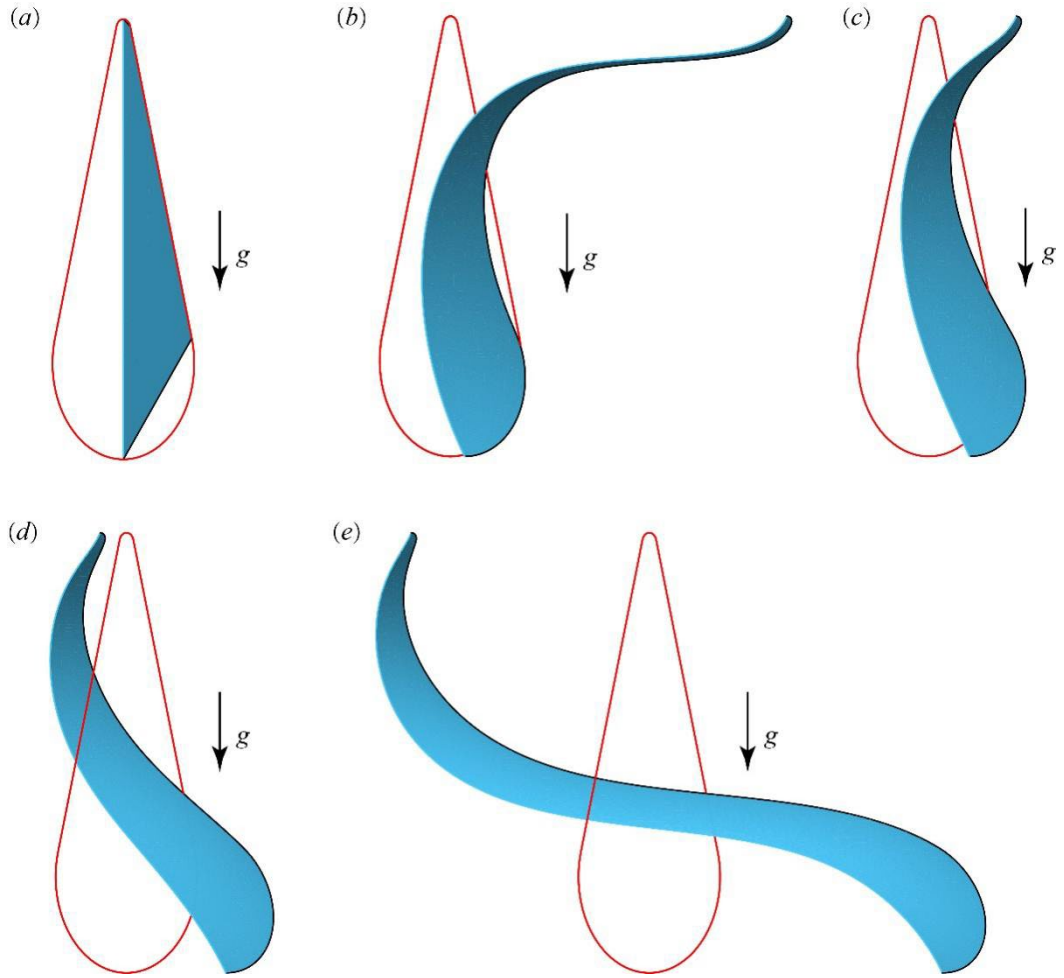

Figure S2. (*a*) The starting geometry, and the solutions at (*b*) Bo = 0.25, (*c*) Bo = 0.394, (*d*) Bo = 0.67, and (*e*) Bo = 0.816 for SE modeling on the case of $\alpha = 30°$ and $r = 0.1$ with $\gamma = 55°$. The red line denotes the cross-section boundary of the tube at $z = 0$. When the computation stopped, the number of facets is 5152 for (*b*), 2567 for (*c*), 2720 for (*d*) and 6731 for (*e*).

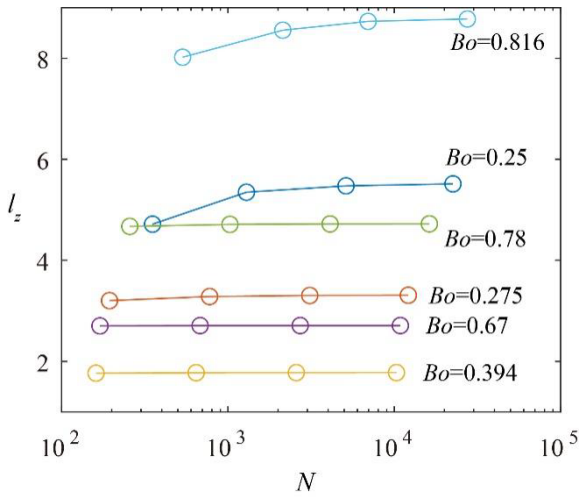

Figure S3. The interface axial length l_z with respect to the number of facets N for the case of $\alpha = 30°$ and $r = 0.1$ with $\gamma = 55°$ at different Bond numbers.

We denote N to be the number of facets. Figure S3 shows the grid dependence on l_z for the case of $\alpha = 30°$ and $r = 0.1$ with $\gamma = 55°$ at different Bond numbers. For $Bo = 0.275$, 0.394, 0.67 and 0.78, when the magnitude of N is larger than 10^2, N has little effect on l_z. However, For $Bo = 0.25$ and 0.816, increasing N from about 300 to a number larger than 2000 leads to an evident increase on l_z. When N is larger than 4000, the change on l_z is small with increasing N.

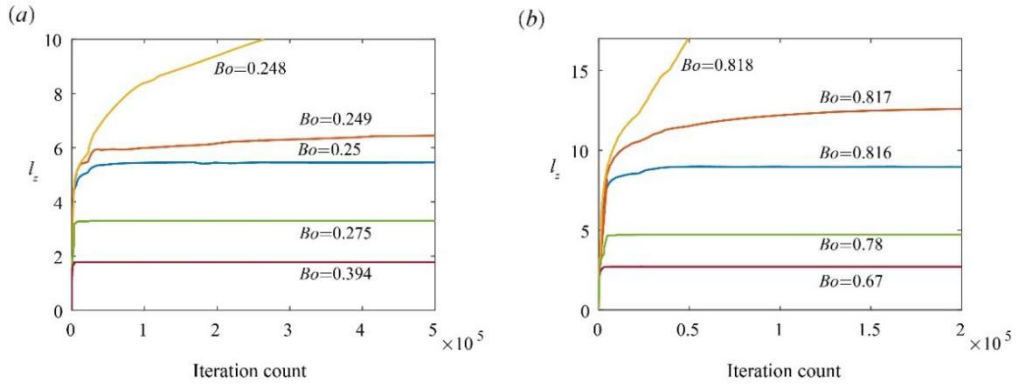

Figure S4. The interface axial length l_z with respect to the iteration count for the case of $\alpha = 30°$ and $r = 0.1$ with $\gamma = 55°$ at (a) small Bond numbers, and at (b) large Bond numbers. In (a), when the computation stopped, the number of facets $N = 2576$ for $Bo = 0.394$, $N = 3104$ for $Bo = 0.275$, $N = 5152$ for $Bo = 0.25$, $N = 5380$ for $Bo = 0.249$, and $N = 5603$ for $Bo = 0.248$. In (b), when the computation stopped, $N = 2720$ for $Bo = 0.67$, $N = 4112$ for $Bo = 0.78$, $N = 6731$ for $Bo = 0.816$, $N = 7923$ for $Bo = 0.817$, and $N = 8392$ for $Bo = 0.818$.

Figure S4 shows the relation between the interface axial length l_z and the number of iterations. When $0.25 \le Bo \le 0.816$, the interface axial length l_z can reach a fixed value after a certain number of iterations. When $Bo \le 0.249$ or $Bo \ge 0.817$, l_z keeps increasing and cannot reach a fixed value even after a large number of iterations, implying that the corresponding computation would diverge and the occluding surface in the tube cannot exist.

For $0.25 \le Bo \le 0.816$, we examine the convergence by investigating the response of the solution to the perturbation. When l_z reaches a fixed value, we exert a 10% elongation on the interface (SE command: set vertex z z*1.1) as a perturbation, and then perform enough iterations to examine if the interface returns to original state or if it diverges. If the perturbed interface can return to the original state, the corresponding original solution is regarded to converge. Figure S5 shows that the change of l_z after perturbation can approach zero after enough iterations, which verifies the convergence of the original solution. For $Bo = 0.275$, 0.394, 0.67 and 0.78, the percent change of l_z approach zero quickly. For $Bo = 0.25$ and 0.816, the percent change of l_z drops from 10% to 2% quickly and then takes a large number of iterations to approach zero.

In conclusion, the minimum and maximum Bond numbers leading to the converge solution of SE modeling are 0.25 and 0.816, respectively, for the case of $\alpha = 30°$ and $r = 0.1$ with $\gamma = 55°$. Therefore, for this case, we determine the SE results for the lower and upper critical Bond numbers for non-occlusion to be 0.25 and 0.816, respectively, which

show good agreement with the theoretical results, i.e. $Bo_{cl} = 0.2474$ and $Bo_{cu} = 0.8183$.

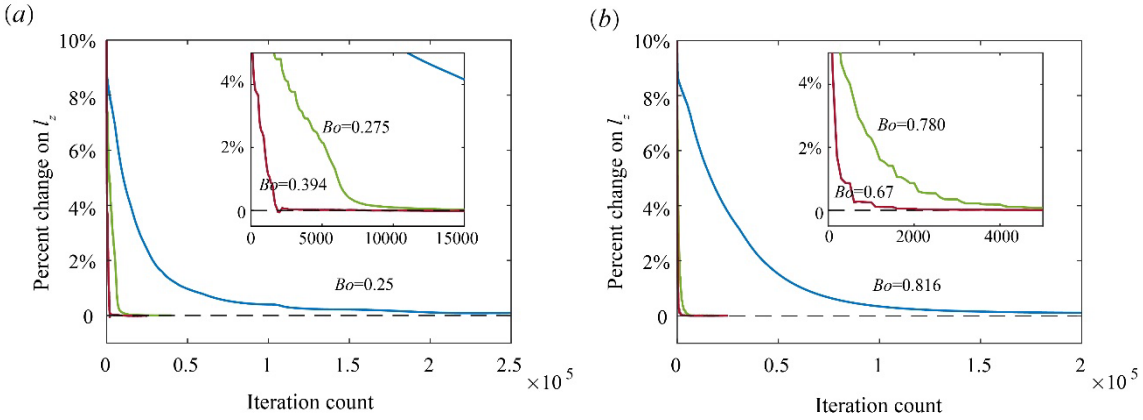

Figure S5. The percentage change on the interface axial length l_z with respect to the iteration count after perturbation for the case of $\alpha = 30°$ and $r = 0.1$ with $\gamma = 55°$ at (*a*) small Bond numbers, and at (*b*) large Bond numbers. The inset in (*a*) shows an enlarged view when the iteration count is between 0 and 15000. The inset in (*b*) shows an enlarged view when the iteration count is between 0 and 6000. In (*a*), when the computation stopped, the number of facets $N = 2576$ for $Bo = 0.394$, $N = 3104$ for $Bo = 0.275$, and $N = 5219$ for $Bo = 0.25$. In (*b*), when the computation stopped, $N = 2720$ for $Bo = 0.67$, $N = 4112$ for $Bo = 0.78$, and $N = 6891$ for $Bo = 0.816$.

References

[1] Brakke, K.A. 2011 Surface Evolver. http://www.susqu.edu/facstaff/b/brakke/.

[2] Chen, Y. 2003 A Study of Capillary Flow in a Vane-Wall Gap in Zero Gravity. Doctoral thesis, Purdue University West Lafayette.